Journal of Molecular Structure 1281 (2023) 135067

Contents lists available at ScienceDirect

Journal of Molecular Structure

journal homepage: www.elsevier.com/locate/molstr

Synthesis of semiconductor ZnO nanoparticles using *Citrus microcarpa* extract and the influence of concentration on their optical properties

A. Villegas-Fuentes[a], H.E. Garrafa-Gálvez[b], R.V. Quevedo-Robles[a], M. Luque-Morales[a,c], A.R. Vilchis-Nestor[d], P.A. Luque[a,*]

[a] Universidad Autónoma de Baja California, Facultad de Ingeniería, Arquitectura y Diseño, C.P. 22860 Ensenada, B.C., México
[b] Universidad Autónoma de Sinaloa, Fuente de Poseidón y Prol. Ángel Flores S/N, C.P. 81223 Los Mochis, Sinaloa, México
[c] Instituto Tecnológico Superior de Guasave, C.P. 81149 Guasave, Sinaloa, México
[d] Centro Conjunto de Investigación en Química Sustentable, UAEM-UNAM, Toluca, México

ARTICLE INFO

Article history:
Received 7 December 2022
Revised 29 January 2023
Accepted 30 January 2023
Available online 31 January 2023

Keywords:
Citrus microcarpa
ZnO
Semiconductor nanoparticles
Synthesis
Organic dye removal

ABSTRACT

In this work, ZnO semiconductor nanoparticles were synthesized by using different concentrations of *Citrus microcarpa* extract 1%, 2%, and 4% w/v (weight/volume), which have organic contents that act as stabilizers in the green synthesis of nanoparticles. The obtained nanoparticles were characterized by several techniques, such as FT-IR, UV-vis, XRD, PL, SEM-EDS, TEM-SAED, and XPS. The FTIR results showed the characteristic vibrations of the extract together with the Zn-O bond ubicated at 480 cm^{-1}; the band gap values decreased as extract concentration increased, obtained 3.03, 2.94, and 2.89 eV for 1%, 2%, and 4% w/v, respectively; XRD and XPS corroborate the formation of ZnO, with a wurtzite phase without impurities as revealed by XRD; PL exhibited a narrow UV emission band and a broader emission band in the visible region; TEM indicates for all product synthesis a quasi-spherical morphology with a decrease in average sizes as the percentage of extract increased being 39.7, 16.8, and 13.1 nm for 1%, 2%, and 4%, respectively. Finally, the photocatalytic activity of the nanoparticles was evaluated by the degradation of Methylene Blue (MB), Methyl Orange (MO), and Rhodamine B (RB) under UV and solar light. The ZnO semiconductor nanoparticles synthesized using 4% extract concentration achieved a 90% degradation of MB during the first 40 and 30 min under UV and solar light, respectively. Additionally, synthesis reached more than 98% of degradation under solar light.

1. Introduction

Nanomaterials have gained considerable attention in recent years and have become one of the most studied fields due to their multidisciplinary nature encompassing a wide variety of applications, among which we can find medicine, catalysis, electronics, optical devices, water treatment, etc. [1]. There are many processes for removing contaminants in wastewater, such as photocatalysis which has positioned itself as an alternative to other methods of contaminant degradation in wastewater due to its efficiency, low toxicity, and simplicity [2]. The efficiency of the photocatalysis it's directly related to the photocatalyst that is being used and its properties, so achieving the desired characteristics such as size, morphology, chemical composition, or crystal structure in the obtainment process is a crucial point [3,4]. Throughout the deep investigations, different materials have been found that are capable of forming nanostructures with unique characteristics, such as silver (Ag) [5], gold (Au) [6], titanium dioxide (TiO_2) [7], tin oxide (SnO_2) [8], iron oxide (Fe_2O_3) [9], and zinc oxide (ZnO) [10]. Among those materials, it stands out ZnO, which is a semiconductor metal oxide with a wide band gap of 3.37 eV and exciton binding energy up to 60 meV [11,12] that has a lot of potential not only by owing superior electrical and optical features like absorbing wavelengths in the UV region, chemical stability, low toxicity, antimicrobial activity, and its ability to form different structures like nanotubes or nanowires, nanoparticles, etc. making ZnO an excellent option in applications like solar cells, nanomedicine, optoelectronics, optical coating, optical sensing, and photocatalysis [13–15]. Some applications of ZnO semiconductor nanoparticles can be found in research, such as Esgin *et al.* (2022) analyzed the photovoltaic performance of Cu-doped ZnO nanopowders as photoanodes for dye sensitized solar cells (DSSC) [16], Fan *et al.* (2022) fabricated a flexible gas sensor based on ZnO nanoparticles decorated with carbon nanofibers to detect ammonia at room temperature [17], or Lahewil *et al.* (2022) syn-

* Corresponding author at: Facultad de Ingeniería, Arquitectura y Diseño-Universidad Autónoma de Baja California, C.P. 22860 Ensenada, Baja California, México.
E-mail address: pluque@uabc.edu.mx (P.A. Luque).

https://doi.org/10.1016/j.molstruc.2023.135067
0022-2860/

thesized ZnO thin films to create structured ultraviolet photodetectors [18]. To synthesize semiconductor ZnO nanoparticles, there are conventional methods widely used, including sol-gel, hydrothermal, spray-pyrolysis, co-precipitation, and thermal decomposition [19,20]; However, these methods have some disadvantages, such as the use of toxic reagents, high pressures, and temperatures, which makes these harmful to the environment [21]. Considering the above, several studies highlight green synthesis as an effective alternative [22]. Green synthesis uses extracts obtained from plants, fruits, leaves, and roots, which, due to their nature, contain active biomolecules, phytochemicals, and secondary metabolites such as terpenoids and flavonoids, which act as stabilizers of a precursor in the synthesis process, favoring the formation and control size of nanoparticles synthesis [23]. Difference of conventional methods, green synthesis has the advantages of not only being friendlier to the environment by not involving conditions or chemicals that become polluting waste; if not that, in many cases, it allows to control of the size and shape of the nanoparticles [24]. According to the literature, some of the extracts have been used in the formation of ZnO nanoparticles, for example, *Lycopersicon esculentum* [25], *Phoenix dactylifera* [26], *Syzygium cumini* [27], *Hibiscus sabdariffa* [28], *Salvia rosmarinus* [29], *Synadenium grantii* [30], *Myristica fragrans* [31]. There is a plant that has not been reported to date for the synthesis of ZnO nanoparticles, the calamansi (*Citrus microcarpa*); this plant is a result of the hybridization of mandarin (*Citrus reticulate*) and kumquat (*Citrus japonica*), it has become popular in North America and Southeast Asia due to its tangerine-like properties and flavor [32]. Different constituent molecules of calamansi have been identified among hydrocarbons (limonene, β-myrcene or β-pinene), terpene alcohols (linalool or elemol), inherent flavonoids, or phenolic acids [33]. These molecules can act as chelating agents to form Zn (II) complexes and as stabilizers during the synthesis process, allowing the formation, growth, and preventing agglomeration of the ZnO nanostructures. In this work, ZnO semiconductor nanoparticles were synthesized using different concentrations of calamansi peel extract, which will be subjected to different characterization tests to determine their physical, chemical, and optical properties. In addition, photocatalysis studies will be carried out to degrade different dyes under UV light and sunlight.

2. Materials and methods

2.1. Materials

For the ecological synthesis of nanoparticles, the materials used were peels of *Citrus microcarpa* as the source of extract, zinc nitrate hexahydrate ($Zn(NO_3)_2{\cdot}6H_2O$) as zinc precursor with a 98% purity was purchased from Sigma-Aldrich and deionized water as reaction media. Furthermore, for the evaluation of the photocatalytic properties, the dyes methylene blue (MB) with a 98% purity, methyl orange (MO) with a 99% purity, and rhodamine B (RB) with a 95% purity; were obtained from Sigma-Aldrich.

2.2. Extracts obtention

To obtain the extracts, peels of *Citrus microcarpa* were dried for 12 h, afterward, grounded and converted to a fine powder. Subsequently, three solutions were prepared at different concentrations, 1%, 2%, and 4%, in a weight-volume relationship in 50 mL of deionized water and placed under constant stirring for 2 h at room temperature. Consecutively, the result solutions were placed in a water bath at 60°C for 1 h. As the last step, the solutions were vacuum filtered with a Whatman No.4 filter paper and stored for further use.

2.3. Synthesis of nanoparticles

For the synthesis of ZnO nanoparticles, 2 g of zinc nitrate hexahydrate was incorporated to the different extract solutions (1%, 2%, and 4%). Then, the solutions were stirred for 1 h until a homogeneous solution was obtained. Subsequently, the different solutions were placed in a thermal bath at 60°C for 12 h until a plastic consistency was obtained. Finally, the samples were calcined at 400°C for 1 h; the powders were collected and labeled as ZnO-1%, ZnO-2%, and ZnO-4% to be stored until used.

2.4. Characterization

Different characterization analyzes were carried out in order to know the physical, chemical, and optical properties of the synthesized materials. To analyze and identify the functional groups and chemical composition of the nanoparticle's powders, Fourier Transform infrared spectra (FTIR) was obtained in a Perkin Elmer spectrophotometer with total attenuated reflectance in a range of 4500 to 350 cm^{-1} in transmittance mode. The optical properties and band gap energy were determined by using ultraviolet-visible spectroscopy (UV-vis); a Lambda 365 Perkin Elmer spectrophotometer was used in this essay. The structural analysis was determined by X-ray diffraction using a Bruker D2-phase diffractometer, Cu K α radiation was used, and a 2θ scanning angle variation between 10° and 80° and a 0.02° step. To obtain the photoluminescence (PL) spectra, a Horiba Nanolog spectrometer was used. Surface morphology and chemical composition were determinate by scanning electron microscopy (SEM) and energy dispersive spectroscopy (EDS), respectively, using a JEOL JSM-6310LV microscope, and the size, shape, and structure of the ZnO nanostructures were determined by using Transmission Electron Microscopy (TEM) with a JEM-2100 microscope from JEOL operated at 200 kV. X-ray photoelectron spectroscopy (XPS) in a SPECS system using monochromatic Al Kα X-rays (1486.6 eV) was used to confirm the chemical and surface composition.

2.5. Photodegradation studies

This essay used a 1:1 relation ratio between nanoparticles and dye solutions (MB, MO, and RB) under UV and solar irradiation conditions. In the typical experiment, 50 mg of ZnO nanoparticles were added to 50 mL of solution at a concentration of 15 ppm of each dye. Subsequently, the suspensions were stirred without light for 30 min, allowing an adsorption/desorption equilibrium of the dye on the nanoparticles surface. The suspensions were exposed to UV light from a 10 W light bulb at 18 mJ/cm^3, and aliquots were taken out at different times until 180 min. On the other hand, a similar experiment was realized using solar light instead of UV. For both experiments, UV and solar, aliquots were taken every 10 min for the first 60 min and then every 30 min until 180 min.

3. Results and discussions

3.1. FTIR analysis

Fig. 1 shows FTIR spectra of ZnO-1%, ZnO-2%, ZnO-4%, and *Citrus microcarpa* extract. The extract shows a strong band at 3300 cm^{-1}, which can be attributed to the bonds of the O-H groups of the alcohols, phenols, and water present; similarly, the band at 1615 cm^{-1} is attributed to O-H stretching [34]. Bands ubicated at 2900 and 2700 cm^{-1} are associated to stretching vibration of C-H bonds [35,36]. Multiple bands can be observed in the region of 1800-900 cm^{-1}, and are attributed to the molecules present in the extract, such as alkaloids, polyphenols, or polyphenols that act as stabilizing agents during the synthesis process [37]. The peak

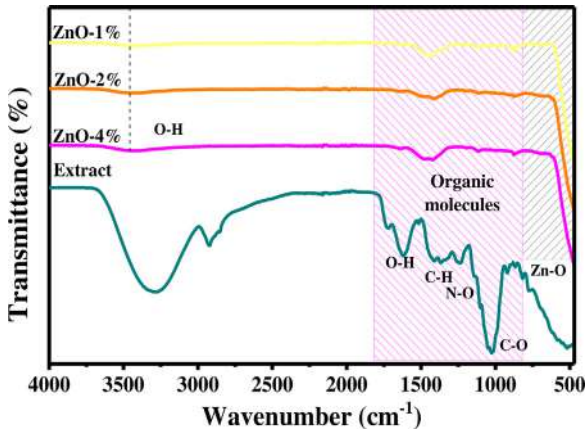

Fig. 1. FTIR spectra of *Citrus microcarpa* extract and ZnO-1%, ZnO-2%, and ZnO-4% nanoparticles synthesized using *Citrus microcarpa* extract.

observed at 1420 cm^{-1} corresponds to the stretching vibration of the C-H bond. Also, the absorption at 1016 cm^{-1} affirms the C-O bond of the aliphatic amines [38]. The bands at 1330, 1080, and 630 cm^{-1} indicate the presence of symmetric N-O narrowing, C-N bonding, and alkyl halides, respectively [39]. Finally, ZnO-1%, ZnO-2%, and ZnO-4% synthesis presented the characteristic band of ZnO ubicated at 480 cm^{-1}, which is attributed to Zn-O vibration, indicating the formation of ZnO [40], along with the characteristic bands of ZnO, some bands were found that are assigned to the organic content of the extracts, as described early. The presence of these bands indicates that the extracts contributed the formation of the ZnO-1%, ZnO-2%, and ZnO-4% nanoparticles.

3.2. UV-vis spectra and bang gap energy

Fig. 2 a shows the absorbance spectra of ZnO-1%, ZnO-2%, and ZnO-4%. For the ZnO-4% sample, the maximum absorbance point is at 364 nm, while for ZnO-1% and ZnO-2%, the maximum absorbance is located at 371 nm; these values are typical of ZnO in works previously reported in the literature, which is assigned to the intrinsic band gap absorption of ZnO [41]. The hypsochromic shift can be attributed to the increase in the concentration of organic matter present in the extract of *Citrus microcarpa*; these differences determine specific properties of each ZnO synthesized [42].

To calculate the band gap of the semiconductor nanoparticles, the TAUC method was used from the UV-vis spectra, using the equation $\alpha(v)h\nu = A(h\nu - E_g)^n$ where $h\nu$ is the energy of the incident photon [43]. E_g is the allowed energy gap, A is a constant, $\alpha(v)$ is the absorption coefficient of the Lambert-Beer Law, and n= 1/2 for allowed direct transition [44,45]. The following procedure was performed. First, the TAUC's equation is compared with the straight-line equation Eq. (1) and (2) by putting the y-axis equal to zero will give us the x-axis Eq. (3), and then solving for the energy, the extrapolation of the first linear region of the plot onto the x-axis, will be the band gap energy Eq. (4).

$$\alpha(v)h\nu = A(h\nu - E_g)^n \quad (1)$$

$$y = m(x) \quad (2)$$

$$0 = A(h\nu - E_g) \quad (3)$$

$$h\nu = E_g \quad (4)$$

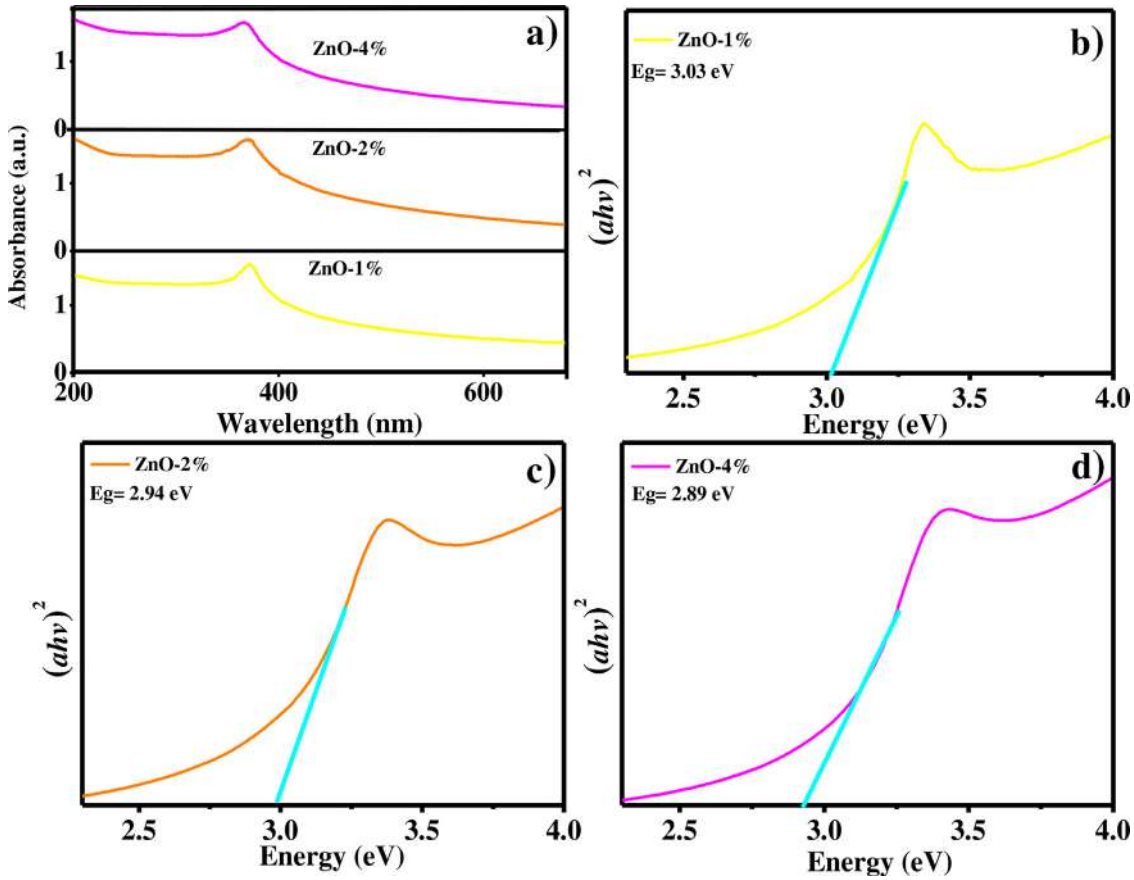

Fig. 2. UV-vis spectra for ZnO-1%, ZnO-2%, and ZnO-4% nanoparticles synthesized using *Citrus microcarpa* a), and TAUC plots for ZnO-1%, ZnO-2%, and ZnO-4%, (b, c, and d, respectively).

The α absorption coefficient is given by the Lambert-Beer law where I is the transmitted light, and I_0 is the incident light Eq. (5). It can also be rearranged and put x=l, which is the thickness of the cell through which the light passes Eq. (6). Using a logarithmic relation on both sides of the equation Eq. (7) [46]. The value of log(e) is 0.4343, so it can be substituted in the equation Eq. (8). By definition $\log(\frac{I_0}{I}) \equiv A$; using the following logarithmic relation $\log(\frac{m}{n}) = -\log(\frac{n}{m})$, the equation could be rearranged Eq. (9) and putting l=1 cm as the standard size of the cuvette the equation is solved Eq. (10) [47,48].

$$I = I_0 e^{-\alpha x} \tag{5}$$

$$\frac{I}{I_0} = e^{-\alpha x} = e^{-\alpha l} \tag{6}$$

$$\log\left(\frac{I}{I_0}\right) = -\alpha l \ \log(e) \tag{7}$$

$$\log\left(\frac{I}{I_0}\right) = -\alpha l \ (0.4343) \tag{8}$$

$$A = -\alpha l \ (0.4343) \tag{9}$$

$$\alpha = 2.302A \ (cm) \tag{10}$$

The incident energy must be converted into units that can be used to calculate the band gap energy (E) Eq. (11). As 1eV= 1.602×10^{-19} J, the equation can be solved as in the equation Eq. (12), as the wavelength in the UV-vis spectrum is nm order, a conversion must be done Eq. (13).

$$E = h\nu = \frac{hc}{\lambda} = \frac{6.625x10^{-34}(Js) * 2.998\ x10^{8}\ \left(\frac{m}{s}\right)}{\lambda\ (m)} \tag{11}$$

$$E = \frac{1.240\ x10^{-6}\ (eV\ m)}{\lambda\ (m)} \tag{12}$$

$$E = \frac{1240\ (eV\ nm)}{\lambda\ (nm)} \tag{13}$$

By using the obtained UV-vis spectrum of the nanoparticles, the x-axis of the TAUC's plot is obtained using Eq. (10). The y-axis is equal to $(\alpha h\nu)^2$ where α is obtained by using the equation Eq. (12) and $h\nu$ is equal to E [49]. As seen in Fig. 2 (b, c, and d) for ZnO-1%, ZnO-2%, and ZnO-4%, the calculated band gaps values were 3.03, 2.94, and 2.89 eV, respectively, the difference with respect to the pristine ZnO (3.37 eV) is due to the organic molecules of the extracts during the synthesis process which results in a slight decrease in the band gap value, a lower band gap value means lower energy to excite the electrons in the valence band to the conduction band which directly affects the photocatalytic activity of the nanoparticles [50].

3.3. X-ray diffraction

Using the XRD technique, the crystalline phase of the ZnO semiconductor nanoparticles were analyzed. Fig. 3 shows the diffraction patterns obtained for ZnO-1%, ZnO-2%, and ZnO-4%. The diffractogram shows well-defined peaks at 31.72°, 34.42°, 36.25°, 47.54°, 56.60°, 62.85°, 66.60°, 67.95°, and 69.11° which correspond to the plans (100), (002), (101), (102), (110), (103), (200), (112), and (201), respectively, this matched with a wurtzite hexagonal phase according to JCPDS crystallographic card No. 36-1451 [51], this confirms the formation of crystalline ZnO semiconductor nanoparticles without impurities or other crystalline phases [52,53]. Then, using the Debye-Scherrer equation Eq. (14), crystallite size was calculated in order to obtain more information about the synthesized material [54]:

$$\tau = \frac{K * \lambda}{\beta * \mathrm{Cos}(\theta)} \tag{14}$$

Where: τ, is the crystallite size; K, is a dimensionless constant with a value of 0.9; λ, is the wavelength of the X-rays; β is the full width at half maximum (FWHM), and θ, is the Bragg's angle in radians [55]. For example, ZnO-1% sample, the values for the calculation of the crystal sizes were the following: K=0.9; λ= 0.1541 nm, for β, of FWHM was 0.2372 which was converted to radians obtaining a value of 4.140×10^{-3}, this value obtained from the 2θ value of 36.24° from which the Bragg angle in radians was ob-

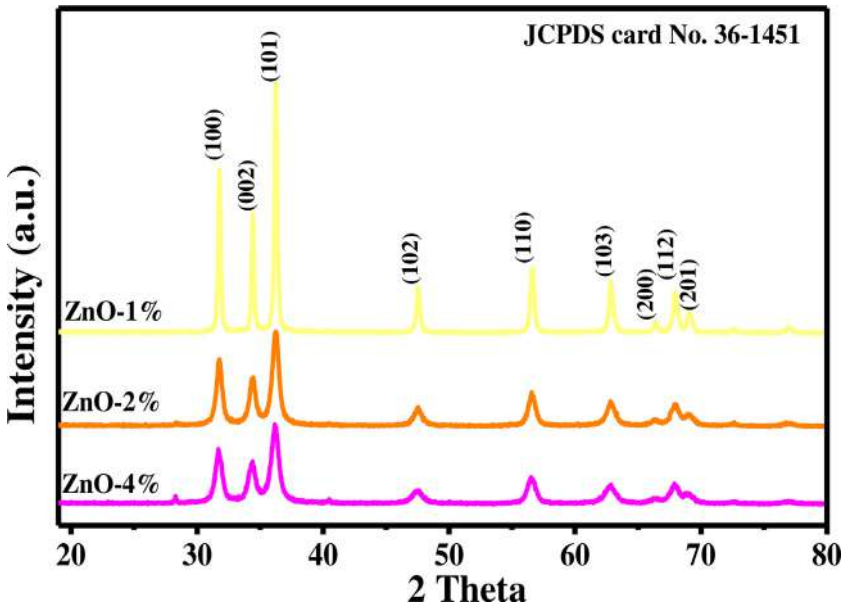

Fig. 3. XRD patterns of the ZnO nanoparticles synthesized using *Citrus microcarpa*.

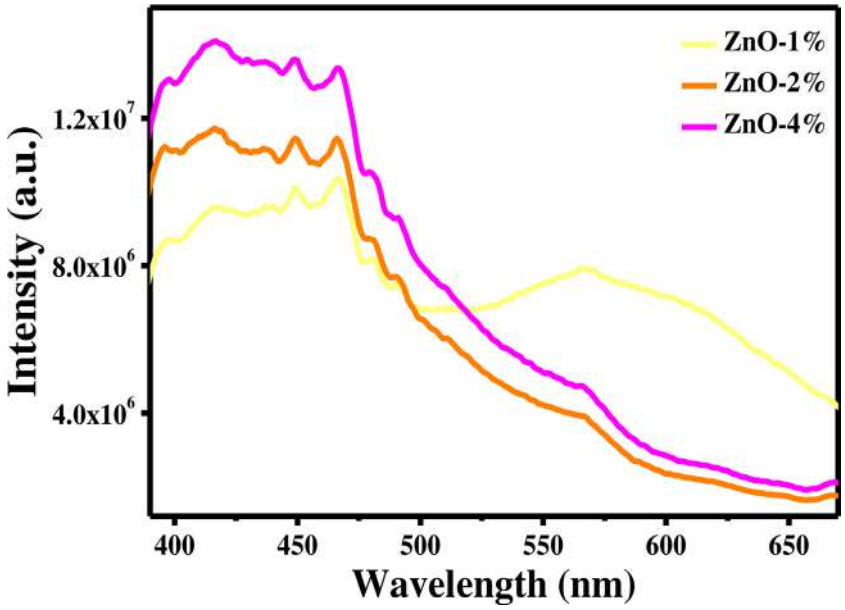

Fig. 4. Photoluminescence spectra of ZnO nanoparticles synthesized using *Citrus microcarpa*.

tained obtaining a value of 0.31625 Eq. (15) [56,57].

$$\tau = \frac{0.9 * 0.1541\ nm}{4.140x10^{-3} * Cos(0.3162)} = 35.24\ nm \quad (15)$$

The same procedure was performed for the ZnO-2% and ZnO-4% samples. The calculated crystal sizes were 35.24, 14.29, and 12.14 nm for ZnO-1%, ZnO-2%, and ZnO-4%, respectively. The results show that when the concentration of the used extract is increased, the crystallite size decreases, which means that the organic content of the *Citrus microcarpa* extracts limits the increase in size; due to improving the capping effect, a similar behavior has been reported in previous investigations [58].

3.4. Photoluminescence

Fig. 4 shows the photoluminescence spectra of ZnO semiconductor nanoparticles synthesized using *Citrus microcarpa* extracts with an excitation wavelength of 370 nm. ZnO-1%, ZnO-2%, and ZnO-4% exhibit a narrow UV emission band and a broader emission band in the visible region. The first band is related to band edge and exciton luminescence, and the second band is attributed to deep-level defects; these bands usually are knowns as near-band edge excitonic (NBE) and deep-level emission (DLE), respectively. The ZnO NPs synthesized present different peaks in the UV-visible region. The peaks centered at 397 nm correspond to the violet region; meanwhile, the bands ubicated in the visible region at 417 nm, 450 nm, 467 nm, 480 nm, 491 nm, and 646 nm were associated with various types of structural defects such as oxygen interstitial and oxygen-interstitial zinc vacancies complexes, lattice defects [59,60].

3.5. SEM and EDX

Fig. 5 (a, b, and c) shows the SEM micrographs of the surface of ZnO-1%, ZnO-2%, and ZnO-4%, all the samples present a quasi-spheric morphology with some agglomeration; however, as the extract concentration is increased a lower agglomeration was observed, as well as a higher dispersion, due to increase in stabilizing molecules present in the extract used in the synthesis process that prevent the agglomeration of nanoparticles. Elemental analysis of the nanoparticles is shown in Fig. 5 (d, e, and f) performed by energy dispersive X-ray spectroscopy. All samples are composed of three elements O, Zn, and C. The signals corresponding to Zn and O indicate the formation and presence of ZnO [61]. The C signals are attributable to the organic matter of the extract used during the synthesis process [62], as previously discussed in FTIR analysis; as a result, it is observed that as the percentage of the extract increases, the atomic percentage of C increases simultaneously.

3.6. Transmission electronic microscopy

Fig. 6 shows the TEM micrographs and SAED patterns of the ZnO-1%, ZnO-2%, and ZnO-4% synthesized using *Citrus microcarpa* extract. All ZnO samples show a quasi-spheric morphology shown in Fig 6. (a, b, and c) with different sizes and small agglomerations for the three syntheses; similar results were reported by Álvarez-Chimal *et al.* (2021) [63]. Fig. 6 (d, e, and f) shows histograms of size distribution of ZnO-1%, ZnO-2%, and ZnO-4%. ZnO-1% presented a distribution size in the range of 20-65 nm, with an average of 39.7 nm. On the other hand, for ZnO-2%, the distribution sizes were between 8 and 22 nm, with an average of 16.8 nm. Meanwhile, the sizes for the ZnO-4% were between 6 and 20 nm, with an average of 13.1 nm. In all three samples, it was observed that as the amount of extract added is increased in the synthesis process, a decrease in the size of the nanoparticles; this confirms a direct relation between the percentage of stabilizers extract molecules and the nanoparticles size preventing the growth of the nanoparticles. This behavior has already been reported in the literature for the green synthesis of semiconductor nanoparticles using plant extract as stabilizing or capping agents [55,64]. Diffraction patterns through TEM were obtained for ZnO-1%, ZnO-2%, and ZnO-4%, which are shown in Fig. 6 (g, h, and i), respectively. The SAED patterns show rings; this indicates the polycrystalline nature of the samples. The rings were assigned to (100), (101), and (102) planes for all three samples; those planes are characteristic of ZnO nanoparticles with a wurtzite structure [65]. The information obtained from SAED studies coincides with the results obtained through XRD, confirming the obtaining of the ZnO nanoparticles with a wurtzite phase.

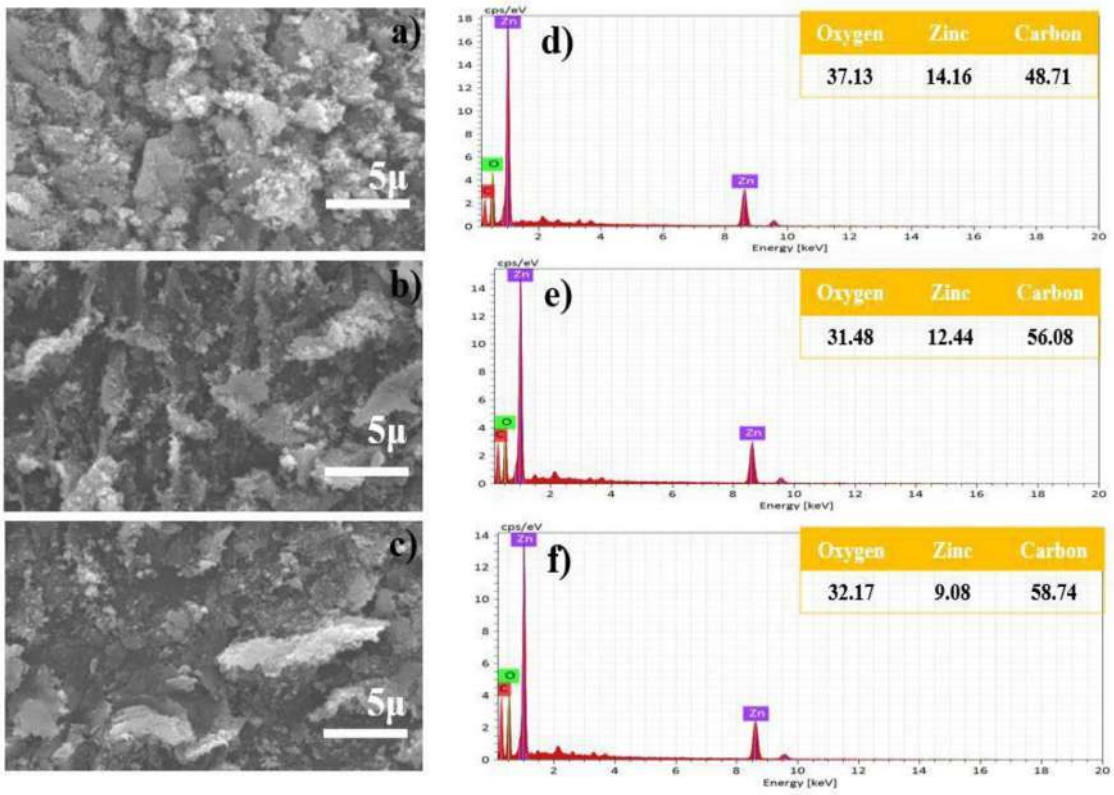

Fig. 5. SEM micrographs of a) ZnO-1%, b) ZnO-2%, and c) ZnO-4%. EDS spectra of d) ZnO-1%, e) ZnO-2%, and f) ZnO-4%.

3.7. XPS analysis

ZnO semiconductor nanoparticles synthesized using different concentrations of *Citrus microcarpa* peel extract were analyzed by XPS, and the results are shown in Fig. 7. First, the analysis of the survey spectrum shown in Fig. 7a indicates that for the different percentages of *Citrus microcarpa* peel extract used, similar peaks were observed, C1s at 284.5 eV; O1s at 529.5 eV; and the main peaks of Zn ($Zn2p_{1/2}$ y $Zn2p_{3/2}$) at 1044 and 1021 eV, respectively. The presence of these peaks directly indicates the obtaining of the ZnO nanoparticles; as reported by Yoon *et al.* (2021), these peaks are characteristic of ZnO nanoparticles [66]. The outstanding peak at 284.5 eV is assigned to C1s due to the carbon content of the organic molecules in the *Citrus microcarpa* extract since the main components are flavonoids, polyphenols, etc., which are largely composed of carbon; this also is a sign that the molecules of the used extract are found in the nanoparticles obtained, previous reports of ZnO nanoparticles derived from plant extracts have demonstrated similar results [67,68].

The high resolution XPS analysis determined similar signals from the three samples; for C1s, a single signal was found without alteration, with a maximum peak at 284.5 eV. In the same way, the O1s presented its peak at 529.5 eV. For the case of the Zn2p peak, a doublet was found at 1044 and 1021 eV, with an energy difference of 23 eV, which are assigned to the Zn^{2+} species, the ZnO samples that present a similar energy difference have been related to the characteristic size of nanoparticles [69].

3.8. ZnO nanoparticles formation mechanism

A mechanism for the ZnO nanoparticles formation is shown in Fig. 8. Biomolecules present in the aqueous extract, such as phenolic compounds, act as chelating agents and stabilizing agents preventing agglomeration. As a result, a stable complex system is formed between the Zn^{2+} ions and the polar groups of the biomolecules; during the calcination, the system undergoes decomposition, leading to the formation of ZnO nanoparticles and by-products released during calcination [70,71].

3.9. Photocatalytic degradation

Fig. 9 shows the results of the photocatalytic degradation of MB under UV and solar light. In both cases, all syntheses showed high photocatalytic activity; however, degradation was faster under sunlight. For ZnO-1% only took 30 min to achieve a 90% degradation, ending with a degradation of 100%; meanwhile, ZnO-2% and ZnO-4% nanoparticles obtained a 100% of degradation at 50 and 40 min, respectively. In the case of the samples that were irradiated with UV light, the ZnO-4% sample presented a better activity and achieved a degradation of 90% in 40 min, while for the ZnO-1% and ZnO-2%, a similar degradation percentage was achieved at 60 min. These results can be related to higher absorption in the visible light region for the ZnO-1% sample, which leads to a higher degradation under solar light.

For RB, Fig. 10 shows the results for both UV and solar degradation. For this dye, photodegradation under solar light occurs faster than UV. The results of the three UV samples, were very similar, removing 93%, 91%, and 90% for the ZnO-1%, ZnO-2%, and ZnO-4%, respectively. On the other hand, in samples exposed under solar light, ZnO-1% showed a faster degradation by removing 92% of the dye at 90 min, while at the same time, the ZnO-2% and ZnO-4% samples had degraded 85% and 89%, respectively. Moreover, all syntheses achieved a 100% of degradation under solar conditions.

MO photodegradation results are shown in Fig. 11; in this case, the photodegradation study realized under UV light showed less degradation than with the other two dyes previously presented, achieving a degradation of 80%, 75%, and 81% for the ZnO-1%, ZnO-2%, and ZnO-4% respectively. In contrast, the degradation under

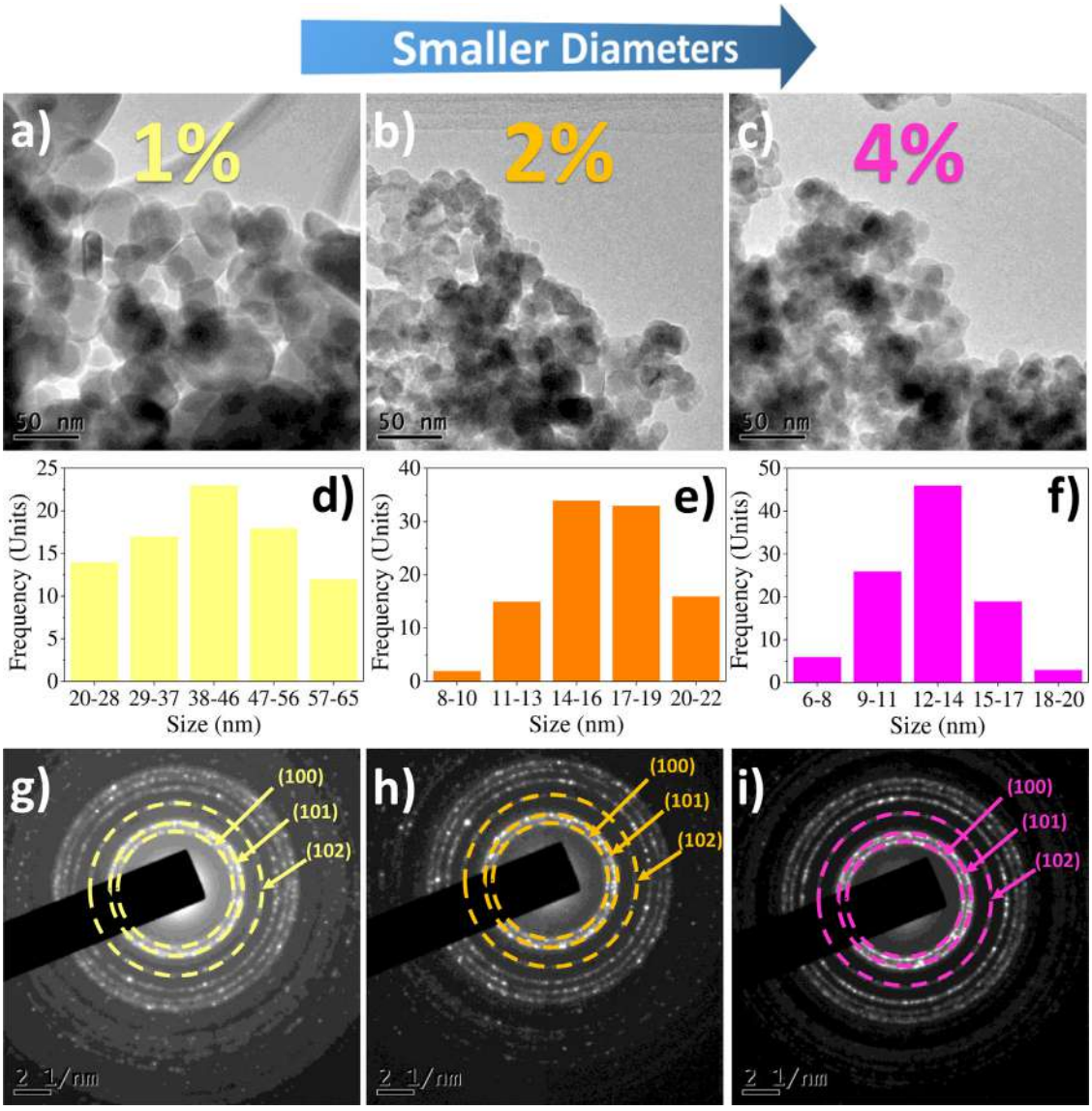

Fig. 6. TEM micrographs, size distribution histograms, and SAED patterns of (a, d, and g) ZnO-1%, (b, e, and h) ZnO-2%, and (c, f, and i) ZnO-4%.

sunlight was improved compared to the solar degradation of MB and RB. The three syntheses presented a 100% final degradation at 180 min.

Table 1 shows the summary of photodegradation percentages of the ZnO-1%, ZnO-2%, and ZnO-4% at 180 min for UV and solar light conditions. For the three dyes, more significant and faster degradation was obtained under sunlight Table 2, especially for the ZnO-1% and ZnO-2% samples, which show a greater absorption in the visible area of the electromagnetic spectrum. MB values greater than 97% were obtained in all photodegradation studies using UV light. Meanwhile, all studies under solar light achieved a 100% degradation; the degradation constant indicates not only greater degradation but also faster for solar light. In the case of RB, all syntheses studied under UV light achieved more than 95% of degradation after 180 min and 100% for solar light; in this case, similar behavior is observed between UV and solar samples where a more significant and faster degradation under solar light takes, the degradation rates confirm the degradation velocity is even more than double in the case of ZnO-1%. In the case of MO, as well as the other two dyes, a trend is seen in which the tests under solar light achieved greater degradation, in which 100% degradation was obtained in all the samples, as described early for the other dyes; however, in the samples under UV light and less degradation is observed unlike, MB or RB in which the highest degradation was for the ZnO-4% sample with 81% degradation.

Table 1
Degradation percentages of the nanoparticles under UV and solar light.

Sample	MB		RB		MO	
	UV (%)	Solar (%)	UV (%)	Solar (%)	UV (%)	Solar (%)
ZnO-1%	98	100	95	100	80	100
ZnO-2%	97	100	98	100	75	100
ZnO-4%	99	100	97	100	81	100

Table 2 shows the degradation constants using the equation $\ln(\frac{C}{C_0}) = kt$, where C_0 is the concentration at t=0, C is the dye concentration, k is the degradation constant, and t is the exposure time.

3.10. Degradation mechanism

Fig. 12 shows a scheme for a degradation mechanism where dye molecules are photodegraded until mineralized. First, when

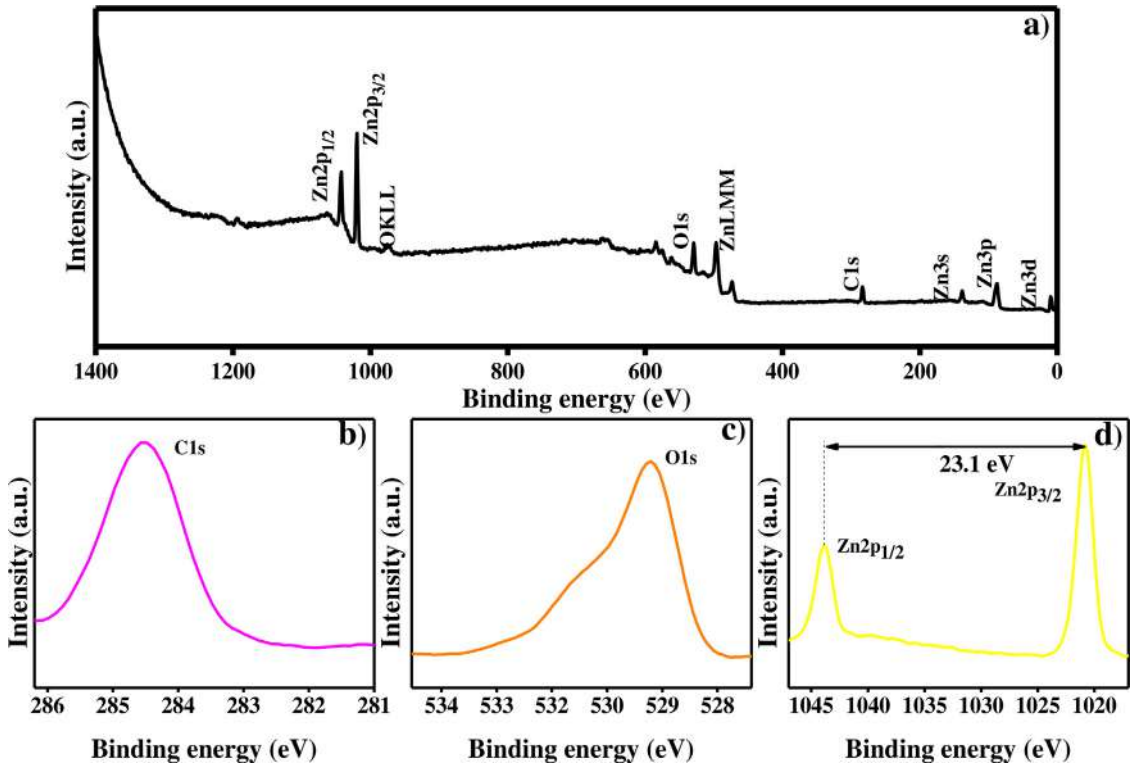

Fig. 7. XPS spectra of ZnO-1%, ZnO-2%, and, ZnO-4% synthesized using *Citrus microcarpa* peel extracts, a) survey scan and high resolution of b) C1s, c) O1s, and d) Zn2p peaks.

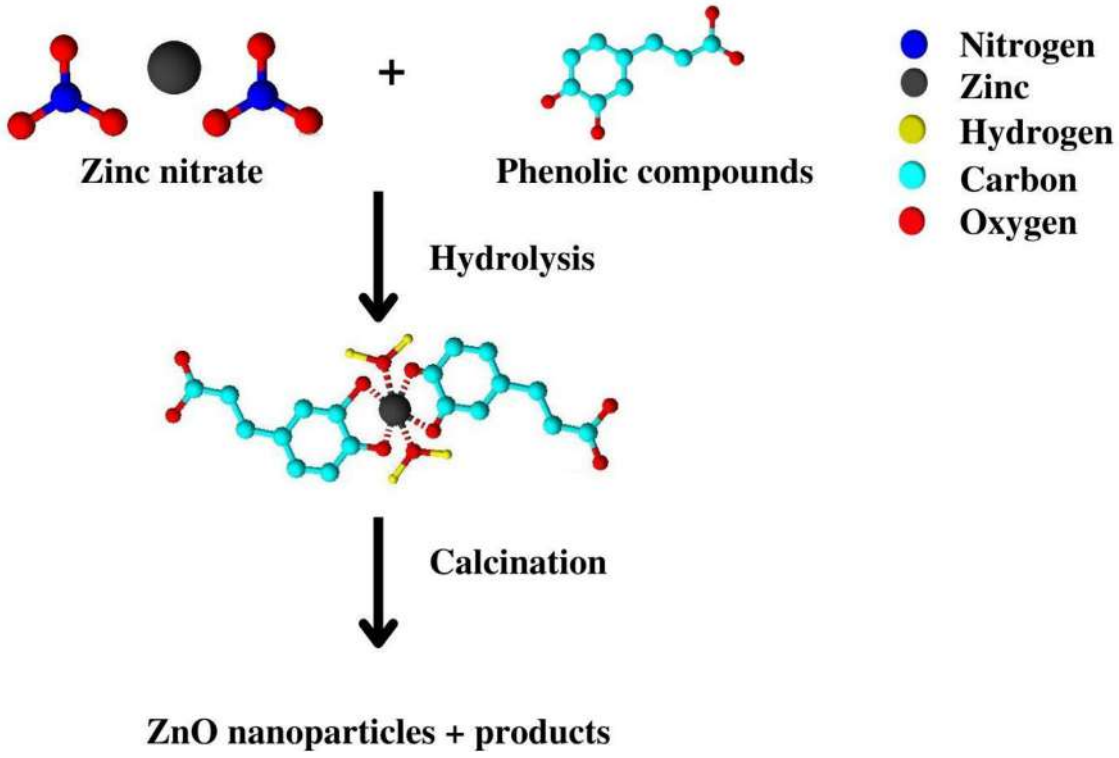

Fig 8. ZnO nanoparticles formation mechanism using green synthesis.

Table 2
Degradation constants *k* of the nanoparticles under UV and solar light.

Sample	MB		RB		MO	
	UV (min^{-1})	Solar (min^{-1})	UV (min^{-1})	Solar (min^{-1})	UV (min^{-1})	Solar ($mirn^{-1}$)
ZnO-1%	0.0287	0.0638	0.0179	0.0491	0.0082	0.0475
ZnO-2%	0.0349	0.0393	0.0204	0.0373	0.0073	0.03085
ZnO-4%	0.0313	0.0355	0.0189	0.0366	0.00906	0.0243

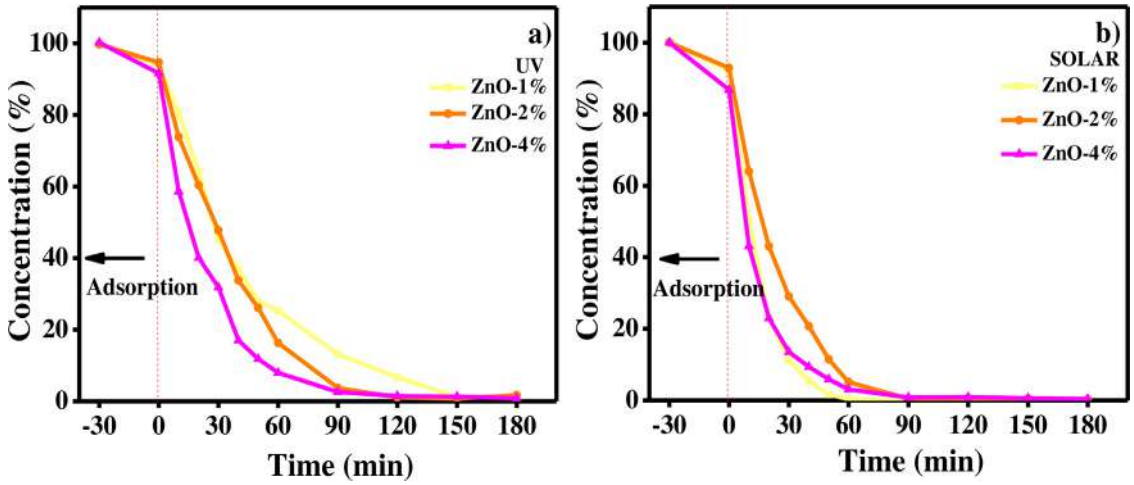

Fig. 9. Photodegradation of MB using ZnO nanoparticles under UV a) and solar b) light.

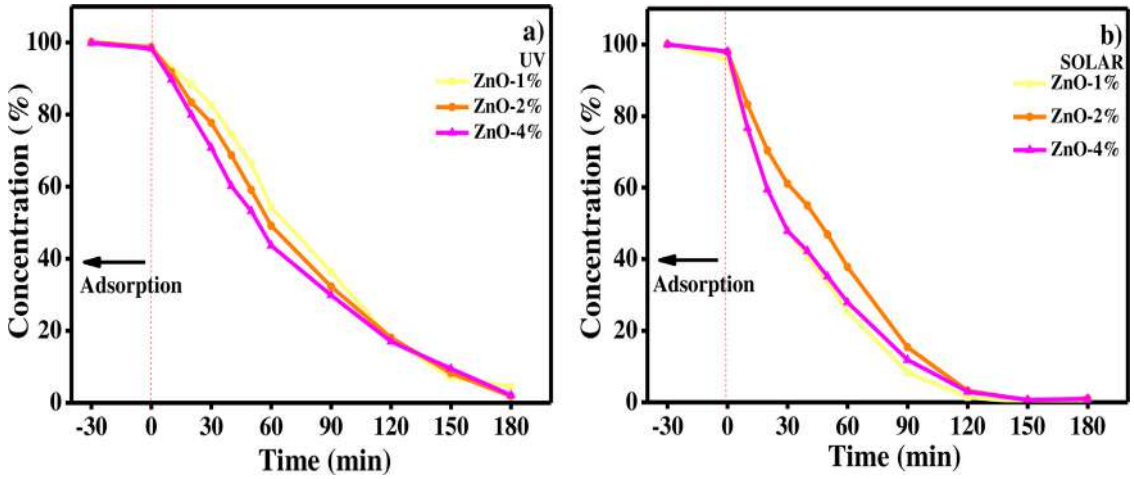

Fig. 10. Photodegradation of RB using ZnO nanoparticles under UV a) and solar b) light.

ZnO semiconductor nanoparticles are irradiated with energy equal o high than the band gap, it causes the excited electrons in the valence band (VB) to be promoted to the conduction band (CB) Eq. (16), generating an electron-hole pair. The hole at the valence band allows the oxidation of H_2O molecules, producing hydroxyl radicals (OH^-) Eq. (17). The electrons at the conduction band reduce the oxygen (O_2) to produce superoxide radicals (O_2^{-}) Eq. (18), which are very reactive and allows to produce more OH^- molecules Eq. (19). Both OH^- and O_2^{-} are reactive and transitory molecules that react with the dye molecules, mineralizing and converting them into less harmful molecules such as H_2O, CO_2, and some other mineral products Eq. (20) and (21) [72].

$$ZnO + h\nu \rightarrow ZnO\ \left(e_{CB}^{-} + h_{VB}^{+}\right) \quad (16)$$

$$h^{+}(VB) + H_2O \rightarrow OH^{\bullet} \quad (17)$$

$$e^{-}(CB) + O_2 \rightarrow\ O_2^{-\bullet} \quad (18)$$

$$O_2^{-\bullet} + H_2O \rightarrow OH^{\bullet} \quad (19)$$

$$O_2^{-\bullet} + dye \rightarrow H_2O + CO_2 + products \quad (20)$$

$$OH^{\bullet} + dye \rightarrow H_2O + CO_2 + products \quad (21)$$

It is shown a comparison of photodegradation studies under UV light using ZnO nanoparticles obtained by using different natural extracts reported in the literature in Table 3. It seeks to make a comparison between the research by highlighting the dye used in the photocatalysis process and its concentration against the degradation time. It can be seen that this work is competent against other investigations by achieving greater degradation in a shorter time at a higher concentration of the dye. The comparison is made only with investigations that carried out the photocatalysis process under UV light because it is easier to compare as it is not affected by environmental factors, unlike the degradations under sunlight.

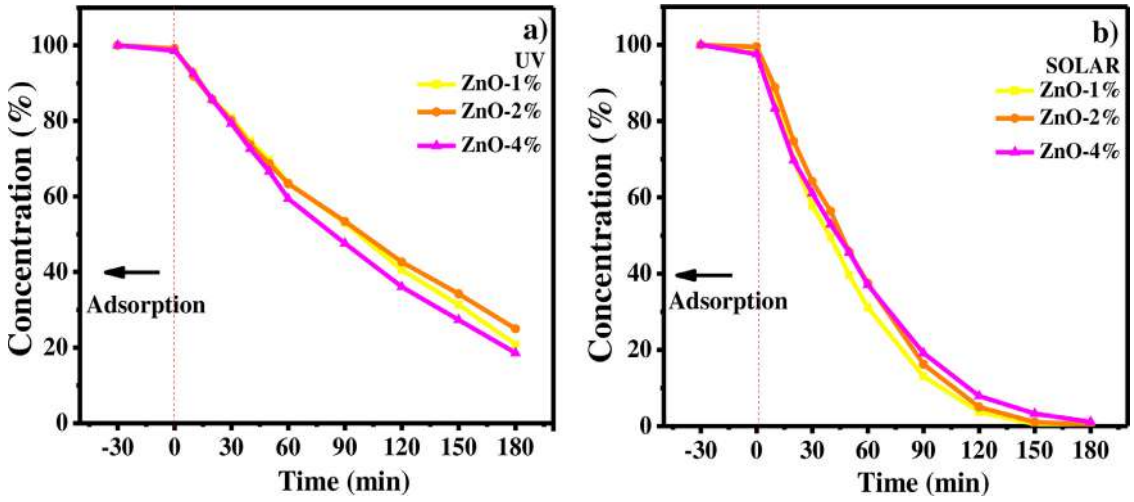

Fig. 11. Photodegradation of MO using ZnO nanoparticles under UV a) and solar b) light.

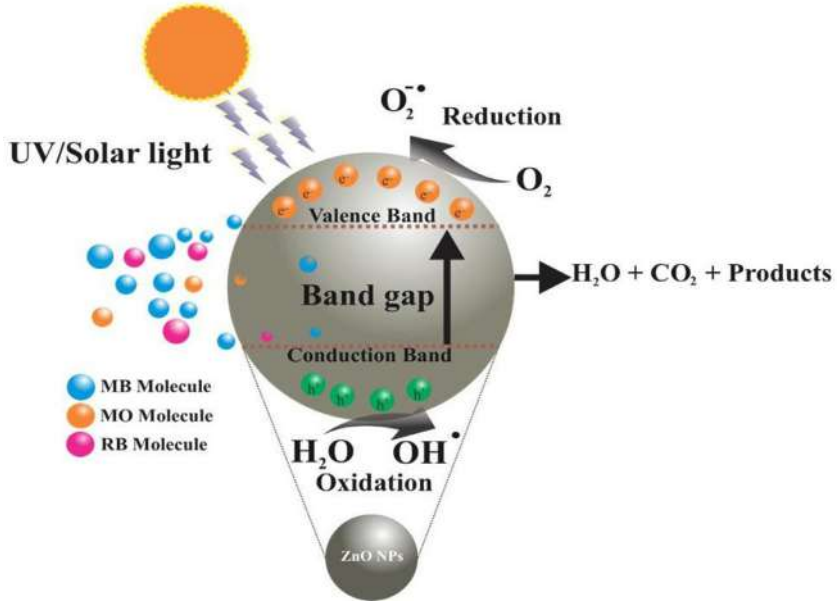

Fig. 12. Photodegradation mechanism of organic dyes using ZnO nanoparticles.

Table 3
Dye degradation using ZnO nanoparticles obtained by green synthesis.

Extract	Dye	Dye concentration	Degradation time	Year	Reference
Citrus microcarpa	MB	15 ppm	120 min (100% degradation)	2023	This work
Citrus microcarpa	MO	15 ppm	180 min (100% degradation)	2023	This work
Citrus microcarpa	RB	15 ppm	180 min (81% degradation)	2023	This work
Phoenix roebelenii	MB	10 ppm	105 min (98% degradation)	2022	[55]
Mussaenda frondosa L.	MB	5 ppm	120 min (90% degradation)	2020	[73]
Coconut husk	MB	5 ppm	100 min (99% degradation)	2021	[74]
Sapindus rarak	RB	0.004 mM	120 min (99% degradation)	2022	[75]
Abelmoschus esculentus	RB	9.5 mg/L	50 min (100% degradation)	2019	[76]
Camellia sinensis	MO	10 mg/L	180 min (80% degradation)	2021	[77]
Salvia officinalis	MO	5 ppm	120 min (92% degradation)	2021	[78]

4. Conclusion

In summary, the synthesis by using *Citrus microcarpa* extract was successful for ZnO semiconductor nanoparticles synthesis in an environmentally friendly way, substituting toxic chemicals with molecules that act as stabilizing agents. The concentration of *Citrus microcarpa* were 1%, 2%, and 4 % w/v, and the percentage variation directly affected on the optical and physical properties of the nanoparticles. FT-IR spectroscopy confirmed the presence of characteristic bands of the organic molecules present in the extract and the Zn-O bond at 480 cm^{-1}. For ZnO-1%, ZnO-2%, and ZnO-4%, the band gap values were 3.03, 2.94, and 2.89 eV, respectively. Crystallite sizes were 35.24, 14.29, and 12.14 nm, respectively; a direct relationship can be observed that by increasing the percentage

of the extract, the band gap value and the crystallite size of the nanoparticles decreases. TEM analysis demonstrates that a higher percentage of extract allows to obtain smaller nanoparticles; the average sizes obtained were 39.7, 16.8, and 13.1 nm for ZnO-1%, ZnO-2%, and ZnO-4%, respectively. XPS and XRD analysis showed characteristic signals of ZnO nanoparticles without alteration in the main peaks or presence of other signals, confirming the chemical composition and the formation of the Zn-O bond. Nanoparticles showed excellent photocatalytic results for the degradation of organic dyes (MB, RB, and MO) under UV and solar light. All samples achieved more than 98% of photodegradation under solar light. For UV and solar light, ZnO-4% degraded 56 and 74% of MB in 60 minutes, respectively, this degradation was superior to others reported in the literature. The physical, chemical, and optical properties of the synthesized ZnO samples show that they could be used not only for photocatalytic applications but for different applications such as sensors, a dopant, or optoelectronic applications.

Declaration of Competing Interest

The authors declare that they have no known financial interests or personal relationships that could influence the submitted work.

CRediT authorship contribution statement

A. Villegas-Fuentes: Conceptualization, Methodology, Writing – review & editing. **H.E. Garrafa-Gálvez:** Conceptualization, Supervision, Validation. **R.V. Quevedo-Robles:** Investigation, Visualization. **M. Luque-Morales:** Methodology, Investigation. **A.R. Vilchis-Nestor:** Investigation, Writing – review & editing. **P.A. Luque:** Conceptualization, Methodology, Resources, Writing – review & editing.

Data availability

Data will be made available on request.

Acknowledgment

This research was financially supported by CONACYT (Grant No. A1-S-34533). We thank to Dr. Uvaldo Hernández (PXRD) and B.Sc. María Citlalit Martínez Soto CCIQS for technical assistance. R.V. Quevedo-Robles acknowledgment CONACyT for postdoctoral scholarship during this study

References

[1] V. Hoseinpour, N. Ghaemi, Green synthesis of manganese nanoparticles: applications and future perspective–a review, J. Photochem. Photobiol. B Biol. 189 (2018) 234–243, doi:10.1016/j.jphotobiol.2018.10.022.
[2] T.U. Doan Thi, T.T. Nguyen, Y.D. Thi, K.H. Ta Thi, B.T. Phan, K.N. Pham, Green synthesis of ZnO nanoparticles using orange fruit peel extract for antibacterial activities, RSC Adv 10 (2020) 23899–23907, doi:10.1039/D0RA04926C.
[3] V.A. Soares, M.J.S. Xavier, E.S. Rodrigues, C.A. de Oliveira, P.M.A. Farias, A. Stingl, N.S. Ferreira, M.S. Silva, Green synthesis of ZnO nanoparticles using whey as an effective chelating agent, Mater. Lett. 259 (2020) 126853, doi:10.1016/j.matlet.2019.126853.
[4] V. Ravichandran, S. Sumitha, C.Y. Ning, O.Y. Xian, U. Kiew Yu, N. Paliwal, S.A.A. Shah, M. Tripathy, Durian waste mediated green synthesis of zinc oxide nanoparticles and evaluation of their antibacterial, antioxidant, cytotoxicity and photocatalytic activity, Green Chem. Lett. Rev. 13 (2020) 102–116, doi:10.1080/17518253.2020.1738562.
[5] A.G. Rama Krishna, C.S. Espenti, Y.V Rami Reddy, A. Obbu, M.V Satyanarayana, Green synthesis of silver nanoparticles by using sansevieria roxburghiana, their characterization and antibacterial activity, J. Inorg. Organomet. Polym. Mater. 30 (2020) 4155–4159, doi:10.1007/s10904-020-01567-w.
[6] J. Singh, T. Dutta, K.-H. Kim, M. Rawat, P. Samddar, P. Kumar, Green' synthesis of metals and their oxide nanoparticles: applications for environmental remediation, J. Nanobiotechnology. 16 (2018) 84, doi:10.1186/s12951-018-0408-4.
[7] B.K. Thakur, A. Kumar, D. Kumar, Green synthesis of titanium dioxide nanoparticles using Azadirachta indica leaf extract and evaluation of their antibacterial activity, South African J. Bot. 124 (2019) 223–227, doi:10.1016/j.sajb.2019.05.024.
[8] K.C. Suresh, S. Surendhiran, P. Manoj Kumar, E. Ranjth Kumar, Y.A.S. Khadar, A. Balamurugan, Green synthesis of SnO_2 nanoparticles using Delonix elata leaf extract: evaluation of its structural, optical, morphological and photocatalytic properties, SN Appl. Sci. 2 (2020) 1735, doi:10.1007/s42452-020-03534-z.
[9] E. Rostamizadeh, A. Iranbakhsh, A. Majd, S. Arbabian, I. Mehregan, Green synthesis of Fe_2O_3 nanoparticles using fruit extract of Cornus mas L. and its growth-promoting roles in Barley, J. Nanostructure Chem. 10 (2020) 125–130, doi:10.1007/s40097-020-00335-z.
[10] S. Fakhari, M. Jamzad, H.Kabiri Fard, Green synthesis of zinc oxide nanoparticles: a comparison, Green Chem. Lett. Rev. 12 (2019) 19–24, doi:10.1080/17518253.2018.1547925.
[11] P. Ramesh, K. Saravanan, P. Manogar, J. Johnson, E. Vinoth, M. Mayakannan, Green synthesis and characterization of biocompatible zinc oxide nanoparticles and evaluation of its antibacterial potential, Sens. Bio-Sensing Res. 31 (2021) 100399, doi:10.1016/j.sbsr.2021.100399.
[12] M.J. Haque, M.M. Bellah, M.R. Hassan, S. Rahman, Synthesis of ZnO nanoparticles by two different methods & comparison of their structural, antibacterial, photocatalytic and optical properties, Nano Express 1 (2020) 010007, doi:10.1088/2632-959x/ab7a43.
[13] S. Annathurai, S. Chidambaram, B. Baskaran, G.K.D. Prasanna Venkatesan, Green synthesis and electrical properties of p-CuO/n-ZnO heterojunction diodes, J. Inorg. Organomet. Polym. Mater. 29 (2019) 535–540, doi:10.1007/s10904-018-1026-1.
[14] Y. Cai, C.B. Yao, Study of well-aligned Ag@ZnO nanoflower arrays with growth, photoluminescence and ultrafast nonlinear absorption properties, Opt. Mater. (Amst). 120 (2021) 111383, doi:10.1016/j.optmat.2021.111383.
[15] M. Ahmad, W. Rehman, M.M. Khan, M.T. Qureshi, A. Gul, S. Haq, R. Ullah, A. Rab, F. Menaa, Phytogenic fabrication of ZnO and gold decorated ZnO nanoparticles for photocatalytic degradation of Rhodamine B, J. Environ. Chem. Eng. 9 (2021) 104725, doi:10.1016/j.jece.2020.104725.
[16] H. Esgin, Y. Caglar, M. Caglar, Photovoltaic performance and physical characterization of Cu doped ZnO nanopowders as photoanode for DSSC, J. Alloys Compd. 890 (2022) 161848, doi:10.1016/j.jallcom.2021.161848.
[17] S.X. Fan, W. Tang, Synthesis, characterization and mechanism of electrospun carbon nanofibers decorated with ZnO nanoparticles for flexible ammonia gas sensors at room temperature, Sensors Actuators B Chem 362 (2022) 131789, doi:10.1016/j.snb.2022.131789.
[18] A.S.Z. Lahewil, S.H. Zyoud, N.M. Ahmed, A.F. Omar, N.Z.N. Azman, Synthesis ZnO nanoclusters micro active area using continues wave blue laser-assisted chemical bath deposition based on UV photodetector, Optik (Stuttg) 260 (2022) 169099, doi:10.1016/j.ijleo.2022.169099.
[19] R. Khosravi, M.H. Ehrampoush, G. Moussavi, M.T. Ghaneian, B. Barikbin, A.A. Ebrahimi, G. Sharifzadeh, Facile green synthesis of zinc oxide nanoparticles using Thymus vulgaris extract, characterization, and mechanism of chromium photocatalytic reduction, Mater. Res. Express. 6 (2019) 115093, doi:10.1088/2053-1591/ab4ae7.
[20] P.A. Luque, O. Nava, C.A. Soto-Robles, M.J. Chinchillas-Chinchillas, H.E. Garrafa-Galvez, Y.A. Baez-Lopez, K.P. Valdez-Núñez, A.R. Vilchis-Nestor, A. Castro-Beltrán, Improved photocatalytic efficiency of SnO_2 nanoparticles through green synthesis, Optik (Stuttg) (2020) 206, doi:10.1016/j.ijleo.2020.164299.
[21] W. Ahmad, D. Kalra, Green synthesis, characterization and anti microbial activities of ZnO nanoparticles using Euphorbia hirta leaf extract, J. King Saud Univ. - Sci. 32 (2020) 2358–2364, doi:10.1016/j.jksus.2020.03.014.
[22] C.A. Soto-Robles, O. Nava, L. Cornejo, E. Lugo-Medina, A.R. Vilchis-Nestor, A. Castro-Beltrán, P.A. Luque, Biosynthesis, characterization and photocatalytic activity of ZnO nanoparticles using extracts of Justicia spicigera for the degradation of methylene blue, J. Mol. Struct. 1225 (2021) 129101, doi:10.1016/j.molstruc.2020.129101.
[23] P.A. Luque, H.E. Garrafa-Gálvez, O. Nava, A. Olivas, M.E. Martínez-Rosas, A.R. Vilchis-Nestor, A. Villegas-Fuentes, M.J. Chinchillas-Chinchillas, Efficient sunlight and UV photocatalytic degradation of Methyl Orange, Methylene Blue and Rhodamine B, using Citrus×paradisi synthesized SnO_2 semiconductor nanoparticles, Ceram. Int. (2021), doi:10.1016/j.ceramint.2021.05.094.
[24] M. Rafique, F. Shafiq, S.S. Ali Gillani, M. Shakil, M.B. Tahir, I. Sadaf, Eco-friendly green and biosynthesis of copper oxide nanoparticles using Citrofortunella microcarpa leaves extract for efficient photocatalytic degradation of Rhodamin B dye form textile wastewater, Optik (Stuttg) 208 (2020) 1–8, doi:10.1016/j.ijleo.2019.164053.
[25] H.E. Garrafa-Galvez, O. Nava, C.A. Soto-Robles, A.R. Vilchis-Nestor, A. Castro-Beltrán, P.A. Luque, Green synthesis of SnO_2 nanoparticle using Lycopersicon esculentum peel extract, J. Mol. Struct. 1197 (2019) 354–360, doi:10.1016/j.molstruc.2019.07.052.
[26] K. Rambabu, G. Bharath, F. Banat, P.L. Show, Green synthesis of zinc oxide nanoparticles using Phoenix dactylifera waste as bioreductant for effective dye degradation and antibacterial performance in wastewater treatment, J. Hazard. Mater. 402 (2021) 123560, doi:10.1016/j.jhazmat.2020.123560.
[27] H. Sadiq, F. Sher, S. Sehar, E.C. Lima, S. Zhang, H.M.N. Iqbal, F. Zafar, M. Nuhanović, Green synthesis of ZnO nanoparticles from Syzygium Cumini leaves extract with robust photocatalysis applications, J. Mol. Liq. (2021) 335, doi:10.1016/j.molliq.2021.116567.
[28] C.A. Soto-Robles, P.A. Luque, C.M. Gómez-Gutiérrez, O. Nava, A.R. Vilchis-Nestor, E. Lugo-Medina, R. Ranjithkumar, A. Castro-Beltrán, Study on the effect of the concentration of Hibiscus sabdariffa extract on the green synthesis of ZnO nanoparticles, Results Phys 15 (2019) 102807, doi:10.1016/j.rinp.2019.102807.

[29] E.R. Silva-Osuna, A.R. Vilchis-Nestor, R.C. Villarreal-Sanchez, A. Castro-Beltran, P.A. Luque, Study of the optical properties of TiO_2 semiconductor nanoparticles synthesized using Salvia rosmarinus and its effect on photocatalytic activity, Opt. Mater. (Amst). 124 (2022) 112039, doi:10.1016/j.optmat.2022.112039.
[30] K.V. Karthik, A.V. Raghu, K.R. Reddy, R. Ravishankar, M. Sangeeta, N.P. Shetti, C.V. Reddy, Green synthesis of Cu-doped ZnO nanoparticles and its application for the photocatalytic degradation of hazardous organic pollutants, Chemosphere 287 (2022) 132081, doi:10.1016/j.chemosphere.2021.132081.
[31] S. Faisal, H. Jan, S.A. Shah, S. Shah, A. Khan, M.T. Akbar, M. Rizwan, F. Jan, N.Akhtar Wajidullah, A. Khattak, S. Syed, Green synthesis of zinc oxide (ZnO) nanoparticles using aqueous fruit extracts of myristica fragrans: their characterizations and biological and environmental applications, ACS Omega 6 (2021) 9709–9722, doi:10.1021/acsomega.1c00310.
[32] M.W. Cheong, D. Zhu, J. Sng, S.Q. Liu, W. Zhou, P. Curran, B. Yu, Characterisation of calamansi (Citrus microcarpa). Part II: volatiles, physicochemical properties and non-volatiles in the juice, Food Chem 134 (2012) 696–703, doi:10.1016/j.foodchem.2012.02.139.
[33] M.W. Cheong, Z.S. Chong, S.Q. Liu, W. Zhou, P. Curran, B. Yu, Characterisation of calamansi (Citrus microcarpa). Part I: volatiles, aromatic profiles and phenolic acids in the peel, Food Chem 134 (2012) 686–695, doi:10.1016/j.foodchem.2012.02.162.
[34] M.W. Amer, A.M. Awwad, Green synthesis of copper nanoparticles by Citrus limon fruits extract, characterization and antibacterial activity, Int. Sci. Organ. 7 (2021) 1–8, doi:10.5281/zenodo.4017993.
[35] H. Ahmad, K. Venugopal, K. Rajagopal, S. De Britto, B. Nandini, H.G. Pushpalatha, N. Konappa, A.C. Udayashankar, N. Geetha, S. Jogaiah, Green synthesis and characterization of zinc oxide nanoparticles using eucalyptus globules and their fungicidal ability against pathogenic fungi of apple orchards, Biomolecules 10 (2020) 1–13, doi:10.3390/biom10030425.
[36] A.S. Abdelbaky, T.A. Abd El-Mageed, A.O. Babalghith, S. Selim, A.M.H.A. Mohamed, Green synthesis and characterization of ZnO nanoparticles using pelargonium odoratissimum (L.) aqueous leaf extract and their antioxidant, antibacterial and anti-inflammatory activities, Antioxidants (2022) 11, doi:10.3390/antiox11081444.
[37] Y. Gao, D. Xu, D. Ren, K. Zeng, X. Wu, Green synthesis of zinc oxide nanoparticles using Citrus sinensis peel extract and application to strawberry preservation: a comparison study, Lwt 126 (2020) 109297, doi:10.1016/j.lwt.2020.109297.
[38] M. Rafique, M. Sohaib, R. Tahir, M.B. Tahir, N.R. Khalid, M. Shakil, S.S.A. Gillani, M.I. Khan, H. Alrobei, K. Shahzad, A.M. Ali, S. Muhammad, Novel, facile and first time synthesis of zinc oxide nanoparticles using leaves extract of Citrus reticulata for photocatalytic and antibacterial activity, Optik (Stuttg) 243 (2021) 167495, doi:10.1016/j.ijleo.2021.167495.
[39] S. Vijayakumar, S. Mahadevan, P. Arulmozhi, S. Sriram, P.K. Praseetha, Green synthesis of zinc oxide nanoparticles using Atalantia monophylla leaf extracts: Characterization and antimicrobial analysis, Mater. Sci. Semicond. Process. 82 (2018) 39–45, doi:10.1016/j.mssp.2018.03.017.
[40] Y.C. Liu, J.F. Li, J.C. Ahn, J.Y. Pu, E.J. Rupa, Y. Huo, D.C. Yang, Biosynthesis of zinc oxide nanoparticles by one-pot green synthesis using fruit extract of Amomum longiligulare and its activity as a photocatalyst, Optik (Stuttg) 218 (2020) 165245, doi:10.1016/j.ijleo.2020.165245.
[41] D.K. Singh, D.K. Pandey, R.R. Yadav, D. Singh, A study of nanosized zinc oxide and its nanofluid, Pramana 78 (2012) 759–766, doi:10.1007/s12043-012-0275-8.
[42] J. Estrada-Urbina, A. Cruz-Alonso, M. Santander-González, A. Méndez-Albores, A. Vázquez-Durán, Nanoscale zinc oxide particles for improving the physiological and sanitary quality of a mexican landrace of red maize, Nanomater 8 (2018), doi:10.3390/nano8040247.
[43] P. Makuła, M. Pacia, W. Macyk, How to correctly determine the band gap energy of modified semiconductor photocatalysts based on UV-Vis spectra, J. Phys. Chem. Lett. 9 (2018) 6814–6817, doi:10.1021/acs.jpclett.8b02892.
[44] J. Sahu, S. Kumar, V.S. Vats, P.A. Alvi, B. Dalela, S. Kumar, S. Dalela, Lattice defects and oxygen vacancies formulated ferromagnetic, luminescence, structural properties and band-gap tuning in Nd^{3+} substituted ZnO nanoparticles, J. Lumin. 243 (2022) 118673, doi:10.1016/j.jlumin.2021.118673.
[45] F.J. Bauer, P.A.B. Braeuer, S. Aßmann, M.A. Thiele, F.J.T. Huber, S. Will, Characterisation of the transition type in optical band gap analysis of in-flame soot, Combust. Flame. 243 (2022) 111986, doi:10.1016/j.combustflame.2022.111986.
[46] Ö.B. Mergen, E. Arda, Determination of optical band gap energies of CS/MWCNT bio-nanocomposites by Tauc and ASF methods, Synth. Met. (2020) 269, doi:10.1016/j.synthmet.2020.116539.
[47] J. Osuntokun, D.C. Onwudiwe, E.E. Ebenso, Green synthesis of ZnO nanoparticles using aqueous Brassica oleracea L. var. italica and the photocatalytic activity, Green Chem. Lett. Rev. 12 (2019) 444–457, doi:10.1080/17518253.2019.1687761.
[48] H. Afzal, M. Ikram, S. Ali, A. Shahzadi, M. Aqeel, A. Haider, M. Imran, S. Ali, Enhanced drug efficiency of doped ZnO-GO (graphene oxide) nanocomposites, a new gateway in drug delivery systems (DDSs), Mater. Res. Express. 7 (2019), doi:10.1088/2053-1591/ab61ae.
[49] B.D. Viezbicke, S. Patel, B.E. Davis, D.P. Birnie III, Evaluation of the Tauc method for optical absorption edge determination: ZnO thin films as a model system, Phys. Status Solidi. 252 (2015) 1700–1710, doi:10.1002/pssb.201552007.
[50] B.T. Sone, E. Makamu, H.E.A. Mohamed, O. Oputu, V. Fester, Green-synthesized ZnO via Hyphaene thebaica fruit extracts: structure & catalytic effect on the ozonation of Coralene Rubine-S2G azo disperse dye, Environ. Nanotechnology, Monit. Manag. 16 (2021) 100515, doi:10.1016/j.enmm.2021.100515.
[51] A. Kumar, Sol gel synthesis of zinc oxide nanoparticles and their application as nano-composite electrode material for supercapacitor, J. Mol. Struct. 1220 (2020) 128654, doi:10.1016/j.molstruc.2020.128654.
[52] B. Janani, A.A. Al-Kheraif, A.M. Thomas, A. Syed, A.M. Elgorban, L.L. Raju, A. Das, S.S. Khan, Construction of nano-heterojunction $AgFeO_2$–ZnO for boosted photocatalytic performance and its antibacterial applications, Mater. Sci. Semicond. Process. 133 (2021) 105924, doi:10.1016/j.mssp.2021.105924.
[53] R. Bekkari, L. Laânab, B. Jaber, Effect of the bivalent dopant ionic radius, electronegativity and concentration on the physical properties of the sol – gel – derived ZnO thin films, J. Mater. Sci. Mater. Electron. 31 (2020) 15129–15139, doi:10.1007/s10854-020-04078-z.
[54] M.B. Perez, C. V Spetter, V.L. Lassalle, Biofabrication of ZnO nanoparticles from Sarcocornia ambigua as novel natural source : a comparative analysis regarding traditional chemical preparation and insights on their photocatalytic activity, 1256 (2022). doi:10.1016/j.molstruc.2022.132460.
[55] T.S. Aldeen, H.E. Ahmed Mohamed, M. Maaza, ZnO nanoparticles prepared via a green synthesis approach: physical properties, photocatalytic and antibacterial activity, J. Phys. Chem. Solids. 160 (2022) 110313, doi:10.1016/j.jpcs.2021.110313.
[56] D. Antony, K. Balasubramanian, R. Yadav, Experimental and computational studies of phytome diate d selenium-CuO and ZnO nanoparticles-potential drugs for breast cancer, J. Mol. Struct. 1263 (2022) 133113, doi:10.1016/j.molstruc.2022.133113.
[57] T. Karnan, S.A.S. Selvakumar, Biosynthesis of ZnO nanoparticles using rambutan (Nephelium lappaceumL.) peel extract and their photocatalytic activity on methyl orange dye, Elsevier Ltd, 2016, doi:10.1016/j.molstruc.2016.07.029.
[58] A.H. Alrajhi, N.M. Ahmed, M. Al Shafouri, M.A. Almessiere, A. ahmed Mohammed Al-Ghamdi, Green synthesis of zinc oxide nanoparticles using salvia officials extract, Mater. Sci. Semicond. Process. 125 (2021) 105641, doi:10.1016/j.mssp.2020.105641.
[59] A. Galdámez-Martinez, G. Santana, F. Güell, P.R. Martínez-Alanis, A. Dutt, Photoluminescence of ZnO nanowires: a review, Nanomaterials 10 (2020), doi:10.3390/nano10050857.
[60] Y. Gong, T. Andelman, G.F. Neumark, S. O'Brien, I.L. Kuskovsky, Origin of defect-related green emission from ZnO nanoparticles: effect of surface modification, Nanoscale Res. Lett. 2 (2007) 297–302, doi:10.1007/s11671-007-9064-6.
[61] A. Ekennia, D. Uduagwu, O. Olowu, O. Nwanji, O. Oje, B. Daniel, S. Mgbii, C. Emma-Uba, Biosynthesis of zinc oxide nanoparticles using leaf extracts of Alchornea laxiflora and its tyrosinase inhibition and catalytic studies, Micron 141 (2021) 102964, doi:10.1016/j.micron.2020.102964.
[62] G. Rashidian, C.C. Lazado, H.H. Mahboub, R. Mohammadi-Aloucheh, M.D. Prokić, H.S. Nada, C. Faggio, Chemically and green synthesized ZnO nanoparticles alter key immunological molecules in common carp (Cyprinus carpio) Skin Mucus, Int. J. Mol. Sci. 22 (2021), doi:10.3390/ijms22063270.
[63] R. Álvarez-Chimal, V.I. García-Pérez, M.A. Álvarez-Pérez, J.Á. Arenas-Alatorre, Green synthesis of ZnO nanoparticles using a Dysphania ambrosioides extract. Structural characterization and antibacterial properties, Mater. Sci. Eng. C. 118 (2021) 111540, doi:10.1016/j.msec.2020.111540.
[64] A. Falih, N.M. Ahmed, M. Rashid, Green synthesis of zinc oxide nanoparticles by fresh and dry alhagi plant, Mater. Today Proc. 49 (2022) 3624–3629, doi:10.1016/j.matpr.2021.08.201.
[65] A. Umamaheswari, S.L. Prabu, S.A. John, A. Puratchikody, Green synthesis of zinc oxide nanoparticles using leaf extracts of Raphanus sativus var. Longipinnatus and evaluation of their anticancer property in A549 cell lines, Biotechnol. Reports. 29 (2021) e00595, doi:10.1016/j.btre.2021.e00595.
[66] J. Yoon, S.-G. Oh, Synthesis of amine modified ZnO nanoparticles and their photocatalytic activities in micellar solutions under UV irradiation, J. Ind. Eng. Chem. 96 (2021) 390–396, doi:10.1016/j.jiec.2021.01.043.
[67] E.F. El-Belely, M.M.S. Farag, H.A. Said, A.S. Amin, E. Azab, A.A. Gobouri, A. Fouda, Green synthesis of zinc oxide nanoparticles (ZnO-nps) using arthrospira platensis (class: Cyanophyceae) and evaluation of their biomedical activities, Nanomaterials 11 (2021) 1–18, doi:10.3390/nano11010095.
[68] J.K. Park, E.J. Rupa, M.H. Arif, J.F. Li, G. Anandapadmanaban, J.P. Kang, M. Kim, J.C. Ahn, R. Akter, D.C. Yang, S.C. Kang, Synthesis of zinc oxide nanoparticles from Gynostemma pentaphyllum extracts and assessment of photocatalytic properties through malachite green dye decolorization under UV illumination-A Green Approach, Optik (Stuttg) 239 (2021) 166249, doi:10.1016/j.ijleo.2020.166249.
[69] Z.Mohamed Riyas, R. Gayathri, M.R. Prabhu, K. Velsankar, S. Sudhahar, Green synthesis and biomedical behavior of Mg-doped ZnO nanoparticle using leaf extract of Ficus religiosa, Ceram. Int. 48 (2022) 24619–24628, doi:10.1016/j.ceramint.2022.05.107.
[70] O.J. Nava, P.A. Luque, C.M. Gómez-Gutiérrez, A.R. Vilchis-Nestor, A. Castro-Beltrán, M.L. Mota-González, A. Olivas, Influence of Camellia sinensis extract on Zinc Oxide nanoparticle green synthesis, J. Mol. Struct. 1134 (2017) 121–125, doi:10.1016/j.molstruc.2016.12.069.
[71] V.V. Gawade, N.L. Gavade, H.M. Shinde, S.B. Babar, A.N. Kadam, K.M. Garadkar, Green synthesis of ZnO nanoparticles by using Calotropis procera leaves for the photodegradation of methyl orange, J. Mater. Sci. Mater. Electron. 28 (2017) 14033–14039, doi:10.1007/s10854-017-7254-2.
[72] M. Samadi, M. Zirak, A. Naseri, M. Kheirabadi, M. Ebrahimi, A.Z. Moshfegh, Design and Tailoring of One-Dimensional ZnO Nanomaterials for Photocatalytic Degradation of Organic Dyes: A Review, Springer, Netherland, 2019, doi:10.1007/s11164-018-03729-5.

[73] M.D. Jayappa, C.K. Ramaiah, M.A.P. Kumar, D. Suresh, A. Prabhu, R.P. Devasya, S. Sheikh, Green synthesis of zinc oxide nanoparticles from the leaf, stem and in vitro grown callus of Mussaenda frondosa L.: characterization and their applications, Appl. Nanosci. 10 (2020) 3057–3074, doi:10.1007/s13204-020-01382-2.

[74] S.S. Priyadharshini, J.P. Shubha, J. Shivalingappa, S.F. Adil, M. Kuniyil, M.R. Hatshan, B. Shaik, K. Kavalli, Photocatalytic degradation of methylene blue and metanil yellow dyes using green synthesized Zinc Oxide (ZnO) nanocrystals, Crystals (2022) 12, doi:10.3390/cryst12010022.

[75] A. Umar, V. Sabrina, Y. Yulizar, Synthesis of ZnO nanoparticles using Sapindus rarak DC fruit pericarp extract for rhodamine B photodegradation, Inorg. Chem. Commun. 141 (2022) 109593, doi:10.1016/j.inoche.2022.109593.

[76] A.R. Prasad, J. Garvasis, S.K. Oruvil, A. Joseph, Bio-inspired green synthesis of zinc oxide nanoparticles using Abelmoschus esculentus mucilage and selective degradation of cationic dye pollutants, J. Phys. Chem. Solids. 127 (2019) 265–274, doi:10.1016/j.jpcs.2019.01.003.

[77] S. MalligArjuna Rao, S. Kotteeswaran, A.M. Visagamani, Green synthesis of zinc oxide nanoparticles from camellia sinensis: organic dye degradation and antibacterial activity, Inorg. Chem. Commun. 134 (2021) 108956, doi:10.1016/j.inoche.2021.108956.

[78] M.A. Abomuti, E.Y. Danish, A. Firoz, N. Hasan, M.A. Malik, Green synthesis of zinc oxide nanoparticles using salvia officinalis leaf extract and their photocatalytic and antifungal activities, Biology (Basel) 10 (2021), doi:10.3390/biology10111075.